International Journal of Heat and Mass Transfer 106 (2017) 861–876

Contents lists available at ScienceDirect

International Journal of Heat and Mass Transfer

journal homepage: www.elsevier.com/locate/ijhmt

Thermal design and operational limits of two-phase micro-channel heat sinks

Sung-Min Kim [a,*], Issam Mudawar [b,*]

[a] School of Mechanical Engineering, Sungkyunkwan University, 300 Cheoncheon-dong, Suwon 400-746, Republic of Korea
[b] Purdue University Boiling and Two-Phase Flow Laboratory (PU-BTPFL), Mechanical Engineering Building, 585 Purdue Mall, West Lafayette, IN 47907-2088, USA

ARTICLE INFO

Article history:
Received 13 August 2016
Received in revised form 5 October 2016
Accepted 6 October 2016
Available online 26 October 2016

Keywords:
Thermal design
Heat sink
Micro-channel
Dryout incipience
Premature critical heat flux
Two-phase critical flow

ABSTRACT

While the vast majority of published studies on two-phase micro-channel heat sinks have been focused on determination of pressure drop and heat transfer coefficient, very few studies have addressed the operational limits of these devices. This study provided a comprehensive methodology for thermal design of micro-channel heat sinks with saturated inlet conditions. This includes predictive methods for pressure drop and heat transfer coefficient using universal correlations that rely on large databases amassed from numerous sources, and which encompass many working fluids, and very broad ranges of hydraulic diameter, mass velocity, inlet pressure, and inlet quality. This is followed by predictive tools for thermal limits associated with dryout incipience and premature critical heat flux, as well as two-phase critical flow limit. The three limits are combined to define an envelope for acceptable heat sink performance. Using these tools, a parametric study is performed to determine the variation of maximum heat flux with total volumetric flow rate for different combinations of the channel's geometrical parameters for three working fluids, HFE-7100, R134a, and water. Then, the values of maximum heat flux are used to assess corresponding variations of pressure drop and maximum bottom wall temperature of the heat sink. It is shown that maximum heat flux is dominated by different limits for different flow rate ranges, and may be increased significantly, while decreasing bottom wall temperature, by using a large number of small channels. Furthermore, using deeper micro-channels is shown to increase maximum heat flux and decrease pressure drop, while producing a relatively weak adverse effect on bottom wall temperature.

1. Introduction

1.1. High-flux two-phase thermal management

As heat dissipation from electronic and power devices began to escalate beyond the capabilities of air cooling technologies and, later, single-phase liquid cooling technologies, thermal management system designers shifted their attention to phase-change cooling technologies, which capitalize on full cooling potential of the working fluid, both sensible and latent [1].

Phase change cooling can be implemented in a variety of configurations, the simplest of which is pool boiling thermosyphons [2–6]. These systems offer several advantages, including simplicity of design, low cost, and, most importantly, passive circulation of the working fluid with the aid of buoyancy. But low circulation speeds place upper limits on cooling performance of thermosyphons that are below the operating heat flux in many cutting-edge electronics applications.

These limits have spurred numerous research efforts aimed at achieving superior cooling performance by capitalizing on high coolant speed achieved with pumped liquid loops. Currently, attention is being placed on three primary competing pumped two-phase cooling schemes: jet-impingement, spray, and micro-channel [7]. Each of these schemes provides intrinsic cooling merits while also posing performance challenges and limits.

Jet impingement provides enormous cooling heat fluxes, but greatly increases coolant flow rate requirements as well as produces appreciable temperature gradients across the heated wall away from the impingement zone [8–10]. To mitigate large temperature gradients, multiple jets have been recommended [11–13] to create multiple impingement zones, but this tactic poses additional challenges, including increased coolant flow rate

* Corresponding authors.
E-mail addresses: smkim@skku.edu (S.-M. Kim), mudawar@ecn.purdue.edu (I. Mudawar).
URLs: http://htl.skku.edu (S.-M. Kim), https://engineering.purdue.edu/BTPFL (I. Mudawar).

http://dx.doi.org/10.1016/j.ijheatmasstransfer.2016.10.020
0017-9310/

Nomenclature

A	base area, $A = W \times L$
Bo	Boiling number, q''_H/Gh_{fg}
C	parameter in Lockhart–Martinelli correlation for boiling flows
Ca	capillary number, $Ca = (\mu_f G)/(\rho_f \sigma)$
C_c	contraction coefficient
$C_{non\text{-}boiling}$	parameter in Lockhart–Martinelli correlation for non-boiling (adiabatic and condensing) flows
c_p	specific heat at constant pressure
D	tube diameter
D_h	hydraulic diameter
f	Fanning friction factor
G	mass velocity
G_c	critical (choking) mass velocity
H_{ch}	micro-channel height
h_{fg}	latent heat of vaporization
h_{tp}	two-phase heat transfer coefficient
k	thermal conductivity
L	device length (also micro-channel length)
m	fin parameter
N	number of micro-channels
P	pressure
P_{crit}	critical pressure
P_F	wetted perimeter of micro-channel
P_H	heated perimeter of micro-channel
P_R	reduced pressure, $P_R = P/P_{crit}$
ΔP	pressure drop
Q_t	total volumetric flow rate
q''	heat flux averaged over base area of heat sink
q''_H	effective heat flux averaged over heated perimeter of micro-channel
q''_{P-CHF}	premature critical heat flux over heated perimeter of micro-channel
Re	Reynolds number
Re_f	superficial liquid Reynolds number, $Re_f = G(1-x)D_h/\mu_f$
Re_{fo}	liquid-only Reynolds number, $Re_{fo} = GD_h/\mu_f$
Re_g	superficial vapor Reynolds number, $Re_g = GxD_h/\mu_g$
Su_{go}	vapor-only Suratman number, $Su_{go} = \rho_g \sigma D_h/\mu_g^2$
T	temperature
v	specific volume
v_{fg}	specific volume difference between saturated vapor and saturated liquid
W	device width (also plenum width)
W_{ch}	micro-channel width
W_s	width of solid sidewall separating micro-channels
$W_{s,e}$	width of endwall of heat sink
We_{fo}	liquid-only Weber number, $We_{fo} = (G^2 D_h)/(\rho_f \sigma)$
We_L	Weber number based on micro-channel's heated length, $We_L = (G^2 L)/(\rho_f \sigma)$
X	Lockhart–Martinelli parameter, $X = \sqrt{(dP/dz)_f/(dP/dz)_g}$
x	thermodynamic equilibrium quality
x_{di}	dryout incipience quality
X_{tt}	Lockhart–Martinelli parameter based on turbulent liquid-turbulent vapor flow, $X_{tt} = (\mu_f/\mu_g)^{0.1}((1-x)/x)^{0.9}(\rho_g/\rho_f)^{0.5}$
z	stream-wise coordinate

Greek symbols

α	void fraction
β	micro-channel aspect ratio ($\beta < 1$)
η	fin efficiency
μ	dynamic viscosity
ρ	density
σ	surface tension
σ_c	area ratio, $(W_{ch}N)/W$
ϕ	two-phase multiplier

Subscripts

A	accelerational
c	contraction
cb	convective boiling dominant heat transfer
e	expansion
F	frictional
f	saturated liquid
fo	liquid only
g	saturated vapor
go	vapor only
in	micro-channel inlet
k	liquid (f) or vapor (g)
max	maximum
nb	nucleate boiling dominant heat transfer
out	micro-channel outlet
sat	saturation
tot	total
tp	two-phase
tt	turbulent liquid-turbulent vapor
tv	turbulent liquid-laminar vapor
vt	laminar liquid-turbulent vapor
vv	laminar liquid-laminar vapor
w	wall

and complex three-dimensional flow instabilities in the expelled liquid.

Spray cooling features superior wall temperature uniformity and reduced coolant flow rate requirements compared to jet-impingement cooling. These merits are realized by breaking the incoming liquid flow into a broad dispersion of small droplets, which greatly increases both the liquid's surface area to volume ratio prior to impact and the fraction of heated wall area directly impacted by liquid [14–20]. A key disadvantage of spray cooling is greatly increased size of electronic module, brought about by the relatively large nozzle-to-wall distance required to ensure liquid breakup. Another disadvantage is the complexity of designing spray cooling modules, given the dependence of cooling performance on an unusually large number of parameters, including thermophysical properties of coolant, inlet pressure, temperature and flow rate, nozzle orifice diameter, spray cone angle, and nozzle-to-surface distance [7].

Two-phase micro-channel cooling is commonly implemented with the aid of a conductive micro-channel heat sink featuring multiple sub-millimeter channels extending between upstream and downstream plenums. Micro-channel heat sinks are very compact and lightweight, provide high heat fluxes, and require minimal coolant inventory [21]. Recent studies have also shown a remarkable versatility of micro-channel heat sinks, including adaptability to passive pumpless loops [22,23], and to implementation in hybrid modules combining the merits of both micro-channel flow and jet impingement [24]. But, like jet-impingement and spray cooling, they pose several drawbacks, including large pressure drop and appreciable axial wall temperature gradients, and the potential for two-phase choking and

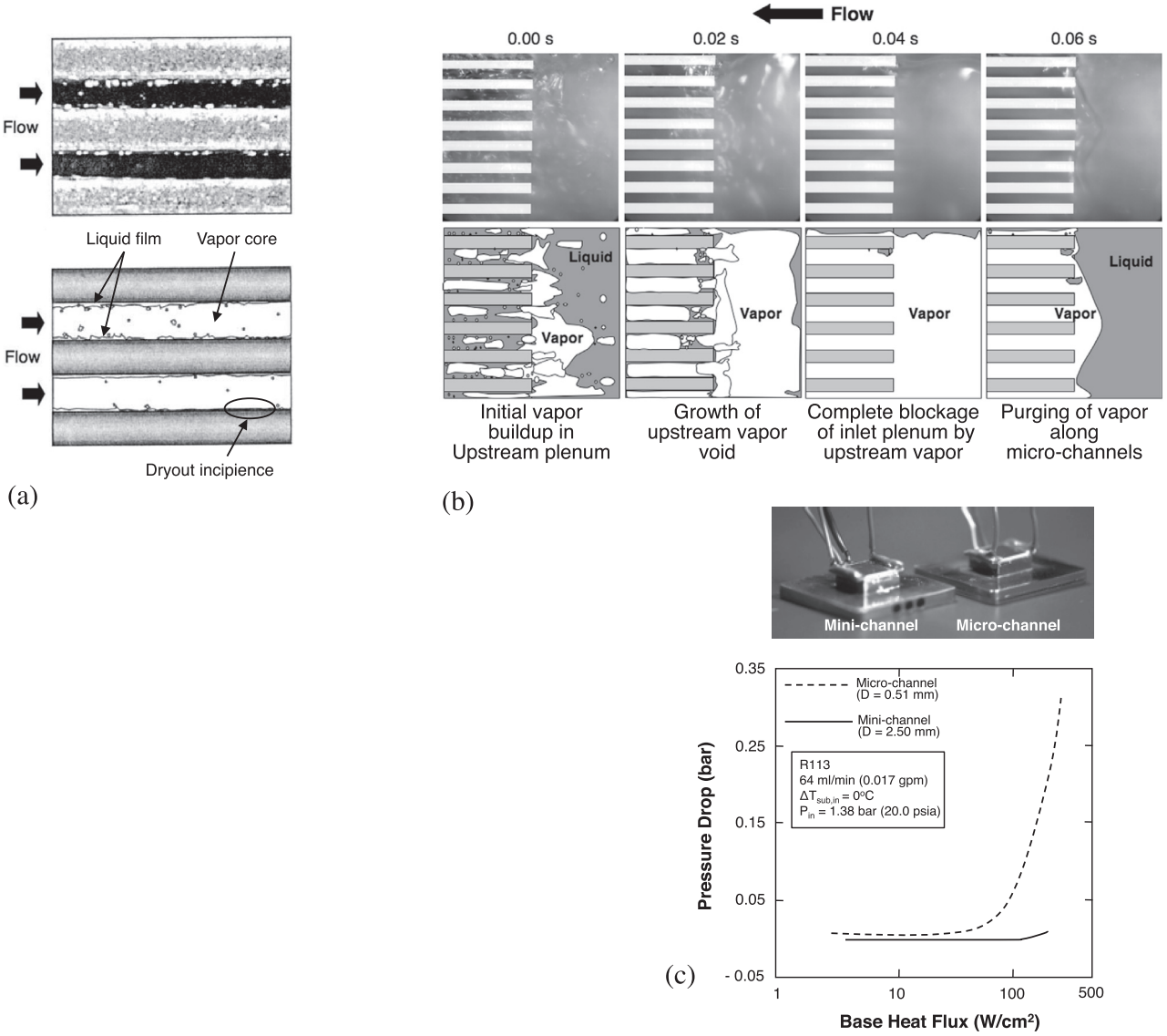

Fig. 1. Design limits for two-phase micro-channel heat sinks. (a) Dryout incipience in R134a for D_h = 348.9 μm, x = 0.68, G = 128 kg/m^2 s, and q'' = 31.6 W/cm^2 [54]. (b) Premature CHF and flow oscillations in HFE-7100 for D_h = 415.9 μm, T_{in} = 0 °C, G = 670 kg/m^2 s, and q'' > 250.0 W/cm^2 [56]. (c) Pressure drop escalation in R113 at high two-phase Mach number in micro-channel heat sink compared to low pressure drop in mini-channel heat sink for identical inlet conditions [57].

premature critical heat flux (CHF) when dissipating high heat fluxes [21]. In fact, these effects set important performance limits that must be carefully assessed when using a two-phase micro-channel heat sink.

The present study concerns predictions of pressure drop and two-phase heat transfer coefficient for two-phase micro-channel heat sinks, including careful assessment of design envelope dictated by the afore-mentioned limits.

1.2. Predictive tools for pressure drop and heat transfer coefficient in two-phase micro-channel heat sinks

Investigators have employed a variety of methods to predict flow boiling pressure drop in micro-channels, which, as discussed in a recent review article by the present authors [25], include theoretical formulations based on the homogeneous equilibrium model [26–31] or empirical and semi-empirical correlations [32–39]; only a few theoretical treatments using the control volume method are presently available (*e.g.*, [40]). Broad utilization of the separated flow model in most recent micro-channel studies is the result of many experimental studies that have shown the dominance of the annular flow pattern for most operating conditions. It should is also noteworthy to mention that the majority of empirical and semi-empirical correlations are based on the original formulation of Lockhart and Martinelli [41] for separated flow.

The authors' recent review article [42] revealed that the vast majority of available predictive methods for two-phase heat transfer coefficient for micro-channel flows are empirical in nature, in which heat transfer is represented by correlations for nucleate boiling, convective boiling, or both [43–48]. Here too, very few theoretical treatments (*e.g.*, [49]) are presently available.

1.3. Dryout and dryout incipience in micro-channels

Critical heat flux is by far the most crucial design and safety parameter for any two-phase scheme used to cool heat-flux-controlled devices, including micro-channel heat sinks. It is the outcome of a substantial reduction in local heat transfer coefficient, brought about by interruption of liquid access to the heated wall. CHF is associated with an unsteady rise in the wall tempera-

ture, the rate of which is dependent on thermophysical properties of the coolant, channel diameter and length, and inlet pressure, inlet quality, and flow rate [50].

Departure from Nucleate Boiling (DNB) is the more catastrophic form of CHF, which is generally encountered with highly subcooled inlet conditions, high mass velocities, and short channels [50–53]. It is triggered by vapor blanket formation along the wall, even where liquid is abundant in the channel core, and manifest by fast escalation in the wall temperature.

Dryout is typically encountered with saturated or slightly subcooled inlet conditions, low mass velocities, and large length-to-diameter ratios, conditions that culminate in early transition to annular flow [54,55]. The annular film is gradually consumed along the channel by interfacial evaporation, and dryout occurs where the film is fully evaporated. Small diameter in micro-channel heat sinks has been shown to cause significant bubble confinement as well as upstream transition to annular flow, which is why CHF in micro-channel heat sinks is associated mostly with dryout rather than DNB [54,55].

Another cooling limit that is especially important to cooling temperature sensitive electronic devices is *dryout incipience*, which is initiated by localized dryout of portions of the annular liquid film, causing substantial reduction in the heat transfer coefficient even upstream of the location of complete dryout. This phenomenon is depicted in Fig. 1(a) for flow boiling of R134a in a micro-channel heat sink [54].

1.4. Premature CHF

Premature CHF is another important design limit inherent to two-phase micro-channel heat sinks, which is triggered by flow instabilities and oscillations. Fig. 1(b) illustrates this phenomenon for the upstream region of a micro-channel heat sink using HFE-7100 as working fluid [56]. It is especially problematic at low mass velocities, which produce high vapor void fractions along the channels. The resulting high pressure drop offers appreciable resistance to the momentum of incoming liquid in the inlet plenum, and causes backflow of vapor from the micro-channels to the inlet plenum. This action blocks incoming liquid from entering the micro-channels, culminating in dryout in the micro-channels. As discussed in [56], two effective means to overcoming premature CHF are to (i) increase mass velocity, to resist the vapor backflow, and (ii) increase inlet subcooling, to reduce the size of vapor void in the inlet plenum.

1.5. Two-phase critical flow

Two-phase flow in micro-channel heat sinks has recently received significant attention for high-flux applications. Small diameter in these devices is key to achieving high heat transfer coefficients. However, small diameter can greatly increase pressure drop, which raises the likelihood of choking.

Pressure drop problems arising from large property variations along the micro-channel heat sink were first addressed and modeled by Bowers and Mudawar [57]. They compared flow boiling of R113 in two heat sinks, one containing circular micro-channels with $D = 0.51$ mm, and the other mini-channels with $D = 2.50$ mm, but both having fairly similar wetted areas. With increasing heat flux, they captured a sharp escalation in pressure drop for the micro-channel heat sink compared to a mild increase for the mini-channel, as shown in Fig. 1(c). High pressure drop in the micro-channel heat sink was attributed to significant compressibility and flashing, caused by large variations of specific volume and enthalpy, respectively, with pressure. The combination of compressibility and flashing also led to large values of two-phase Mach number, raising the potential for two-phase choking. It is important to note that choking is far more prevalent in two-phase than single-phase systems because critical (sonic) speed for a two-phase liquid–vapor mixture is much smaller than that of pure liquid or pure vapor. This implies choking may constitute a serious design limit for two-phase micro-channel heat sinks. In a recent study, the present authors examined relationships among two-phase critical flow, premature CHF, and CHF for micro-channel heat sinks, and showed how choking can trigger premature CHF and/or CHF at low pressures, especially for very small channel diameters [58].

1.6. Objectives of study

This study is the culmination of a series of studies that have been recently performed at the Purdue University Boiling and Two-Phase Flow Laboratory (PU-BTPFL) in pursuit of accurate predictive tools for two-phase micro-channel heat sinks. They include universal correlations for two-phase pressure drop [59], dryout incipience [60], and two-phase heat transfer coefficient [61], as well as predictive methods for premature CHF [62] and two-phase critical flow [58]. A clear distinction must be made between universal correlations and the majority of correlations available from the literature. Most correlations are limited to a single working fluid or a few fluids, and narrow ranges of geometrical or operating parameters, which greatly compromises their effectiveness as design tools. On the other hand, universal correlations derive

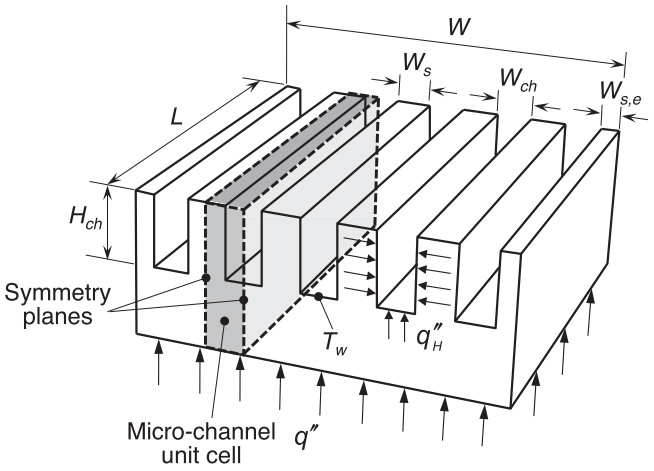

Fig. 2. Schematic of micro-channel heat sink with three-sided wall heating.

Table 1
Design parameters and constraints used in the present study.

	Parameter	Value
Heat sink	Flow direction	Horizontal
	Heated width, W	1 cm
	Heated length, L	1 cm
	Base area, $A = W \times L$	1 cm^2
	Flow geometry	Horizontal rectangular
	Channel height, H_{ch}	400, 800 μm
	Channel width, W_{ch}	$40 \leqslant W_{ch} \leqslant 1000$ μm
	Width of solid sidewall, W_s	$W_s \geqslant 40$ μm
	Width of endwall, $W_{s,e}$	$0.5\ W_s \leqslant W_{s,e} \leqslant 1.0\ W_s$
	Thermal conductivity of oxygen-free cooper, k	391 W/m·K
Operating conditions	Channel inlet pressure, P_{in}	3 bar
	Channel inlet quality, x_{in}	0.05
	Working fluids	HFE-7100, R134a, water

their effectiveness and predictive accuracy from reliance on large databases amassed from numerous sources, and encompassing many working fluids, and very broad ranges of hydraulic diameter, mass velocity, inlet pressure, and inlet quality.

Using the above-mentioned design tools for saturated flow boiling in micro-channel heat sinks, the primary objectives of the present study are to:

(1) Provide optimum predictive methods for total pressure drop across micro-channel heat sink, which dictates pumping power requirements.
(2) Provide optimum predictive methods for two-phase heat transfer coefficient in micro-channel heat sinks, which is required to predict maximum heat sink temperature, and ensure that the heat sink design is capable of maintaining device temperature safely below its maximum allowable limit.
(3) Provide optimum predictive methods for heat sink heat transfer limits of dryout incipience and premature CHF, and flow limit of two-phase critical flow.
(4) Conduct a parametric study to assess various influences on pressure drop, maximum heat sink temperature, and both heat transfer and flow limits in pursuit of superior heat sink design.

2. System parameters and predictive methods

2.1. Heat sink geometry, working fluids, and operating conditions

Fig. 2 shows a schematic of the two-phase micro-channel heat sink geometry examined in this study, which is also the configuration most widely used in practical electronic cooling packages. The heat sink has a fixed base area of width $W = 1$ cm and length $L = 1$ cm, and contains multiple micro-channels. The parametric study will allow for varying dimensions of channel height, H_{ch}, channel width, W_{ch}, width of solid wall between micro-channels, W_s, and width of endwall, $W_{s,e}$. The heated width of heat sink, W, can be related to the number of micro-channels, N, in the heat sink according to

$$W = NW_{ch} + (N-1)W_s + 2W_{s,e}. \tag{1}$$

In this parametric study, the maximum value of W_{ch} is set at 1000 μm, and minimum values of both W_{ch} and W_s at 40 μm. Oxygen-free copper, with $k = 391$ W/m·K, is assumed for heat sink material. All calculations are conducted using a fixed channel inlet pressure of 3 bar, and a fixed inlet quality value of 0.05, meaning the flow enters the micro-channels as a saturated two-phase mixture. To account for performance variations resulting from thermophysical properties, three different working fluids are considered: HFE-7100, R134a, and water. Values or ranges of the heat sink's geometrical parameters are provided in Table 1, while Table 2 summarizes saturated thermophysical properties of the three working fluids corresponding to the inlet pressure of 3 bar. Despite the specific limits adopted in this study and specific fluids examined, the primary goal is to assess the influence of key geometrical parameters on heat sink performance, while, simultaneously, provide a systematic methodology the reader may follow to address other fluids or operating conditions of interest.

In what follows, predictive methods are provided for pressure drop and heat transfer coefficient, followed by important limits associated with dryout incipience, premature CHF, and two-phase critical flow.

2.2. Total pressure drop

Total pressure drop between the heat sink's upstream and downstream plenums is the sum of pressure drop contributions of inlet contraction, ΔP_c, saturated flow boiling region, ΔP_{tp}, and outlet expansion, ΔP_e,

$$\Delta P_{tot} = \Delta P_c + \Delta P_{tp} + \Delta P_e. \tag{2}$$

The contraction pressure loss and expansion recovery at the inlet and outlet of the micro-channels are determined according to [63]

$$\Delta P_c = \frac{G^2 v_f}{2}\left[\left(\frac{1}{C_c} - 1\right)^2 + (1-\sigma_c^2)\right]\left[1 + \frac{v_{fg}x_{in}}{v_f}\right] \tag{3}$$

$$\text{and} \qquad \Delta P_e = G^2\sigma_c(\sigma_c - 1)v_f\left[1 + \frac{v_{fg}x_{out}}{v_f}\right], \tag{4}$$

respectively. In the above equations, plenum height is set equal to the micro-channel height, thus the area ratio is given by

$$\sigma_c = \frac{W_{ch}N}{W}. \tag{5}$$

Additionally, the flow quality is assumed equal to the thermodynamic equilibrium quality, and this assumption is used in all subsequent equations. Based on recommendations by Schmidt and Friedel [64] and Abdelall et al. [65], the vena-contracta effect can be neglected for saturated inlet conditions, allowing the contraction coefficient in Eq. (3) to be set at $C_c = 1$.

For horizontal channels, gravitational pressure drop is neglected and the two-phase pressure drop can be expressed as the sum of accelerational and frictional components,

$$\Delta P_{tp} = \Delta P_{tp,A} + \Delta P_{tp,F}. \tag{6}$$

The accelerational pressure gradient is given by

$$-\left(\frac{dP}{dz}\right)_A = G^2\frac{d}{dz}\left[\frac{v_g x^2}{\alpha} + \frac{v_f(1-x)^2}{(1-\alpha)}\right], \tag{7}$$

where the void fraction, α, is expressed in terms of quality using Zivi's relation [66],

$$\alpha = \left[1 + \left(\frac{1-x}{x}\right)\left(\frac{\rho_g}{\rho_f}\right)^{2/3}\right]^{-1}. \tag{8}$$

The two-phase frictional pressure drop, $\Delta P_{tp,F}$, is both a major contributor to total pressure drop and the most elusive of all pressure drop components. In the present study, $\Delta P_{tp,F}$ is determined using the authors' universal pressure drop correlation [59] for mini/micro-channels. This universal correlation is derived from a

Table 2
Thermophysical properties of saturated HFE-7100, R134a, and water at $P_{sat} = 3$ bar.

	T_{sat} [°C]	ρ_f [kg/m^3]	ρ_g [kg/m^3]	μ_f [kg/m s]	h_f [kJ/kg]	h_{fg} [kJ/kg]	k_f [W/m K]	$c_{p,f}$ [J/kg K]	σ [mN/m]
HFE-7100	98.7	1258	27.7	2.48×10^{-4}	140.1	98.4	0.0545	1330	7.5
R134a	0.70	1293	14.8	2.64×10^{-4}	200.9	198.1	0.0917	1343	11.5
Water	133.5	932	1.65	2.07×10^{-4}	561.4	2164	0.6837	4269	52.2

Table 3
Summary of key predictive methods used in the present study.

	Equation	Remarks
Frictional pressure gradient [59]	$\left(\frac{dp}{dz}\right)_F = \left(\frac{dp}{dz}\right)_f \phi_f^2$ where $\phi_f^2 = 1 + \frac{C}{X} + \frac{1}{X^2}$, $X^2 = \frac{(dp/dz)_f}{(dp/dz)_g}$, and C is determined from Eqs. (16a) and (16b)	• $0.349 < D_h < 5.35$ mm • Fluids: FC-72, R12, R134a, R22, R245fa, R410A, ammonia, CO_2, and water • Universal correlation based on 2378 data points from 16 sources
Heat transfer coefficient for saturated flow boiling [61]	$h_{tp} = \left(h_{nb}^2 + h_{cb}^2\right)^{0.5}$ where h_{nb} and h_{cb} are determined from Eqs. (24a) and (24b), respectively	• $0.19 < D_h < 6.5$ mm • Fluids: FC-72, R11, R113, R123, R1234yf, R1234ze, R134a, R152a, R22, R236fa, R245fa, R32, R404A, R407C, R410A, R417A, CO_2, and water • Universal correlation based on 10,805 pre-dryout data points from 37 sources
Dryout incipience [60]	$x_{di} = 1.4We_{fo}^{0.03}P_R^{0.08} - 15.0(Bo\frac{\mu_g}{\mu_f})^{0.15}Ca^{0.35}\left(\frac{\rho_g}{\rho_f}\right)^{0.06}$	• $0.51 < D_h < 6.0$ mm • Fluids: FC-72, R113, R1234yf, R1234ze, R134a, R22, R245fa, R290, R32, R407C, R410A, CO_2, and water • Universal correlation based on 997 data points from 26 sources
Premature critical heat flux [62]	$q''_{P-CHF} = 33.43Gh_{fg}\left(\frac{\rho_g}{\rho_f}\right)^{1.11}We_L^{-0.21}\left(\frac{L}{D_h}\right)^{-0.36}$	• $D_h = 341$ μm for water (three-sided heated) • $D = 2.54$ mm, 510 μm for R113
Two-phase critical flow [58]	$G_c = \left\{-\left[x\frac{dv_g}{dP} + (1-x)\frac{dv_f}{dP}\right]\right\}^{-0.5}$	• $1.33 < D < 5.4$ mm • Fluids: water, R134a, air–water • Choking data through pipes, short tube orifices, and short nozzles

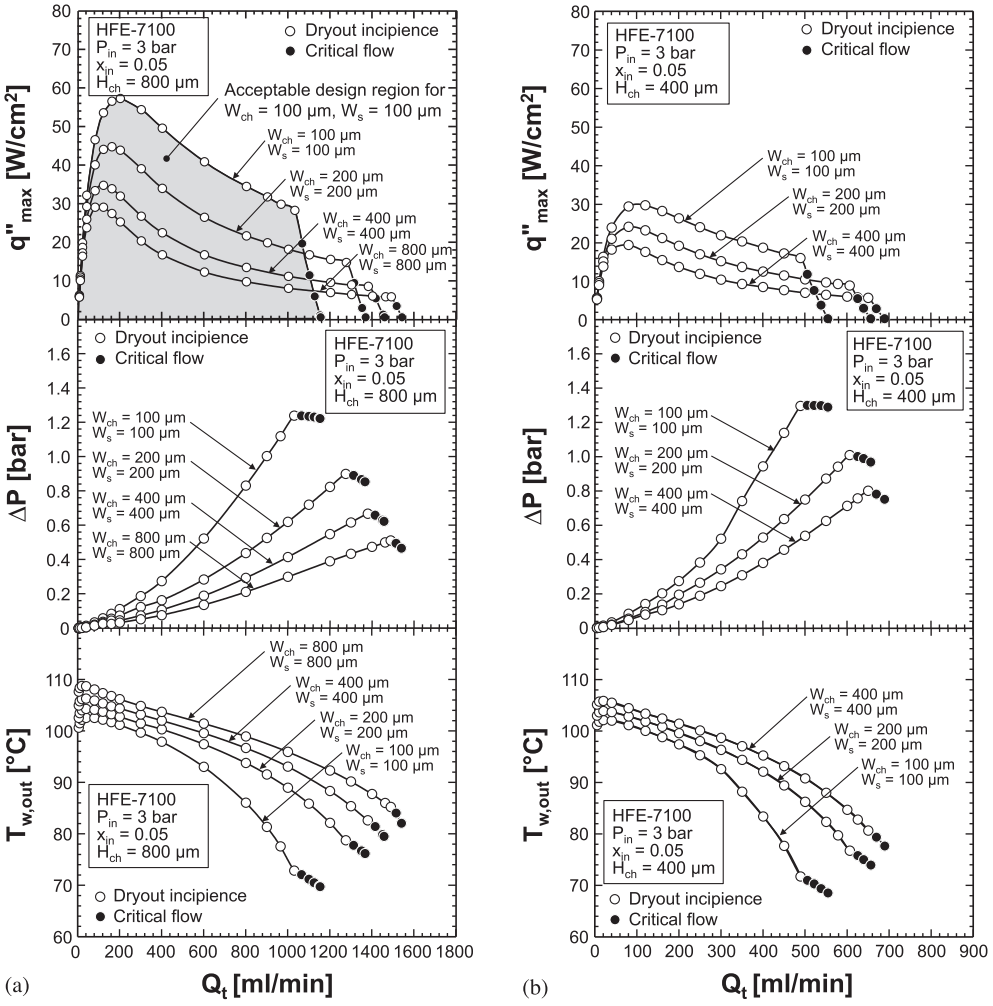

Fig. 3. Variations of maximum base heat flux and corresponding values of total pressure drop and bottom wall temperature at channel exit with total volume flow rate for different channel widths and sidewall thicknesses using HFE-7100 as working fluid: (a) H_{ch} = 800 μm and (b) H_{ch} = 400 μm.

database consisting of 2378 data points amassed from 16 sources. The database consists of 9 working fluids, hydraulic diameters from 0.349 to 5.35 mm, mass velocities from 33 to 2738 kg/m^2 s, liquid-only Reynolds numbers from 156 to 28,010, qualities from 0 to 1, reduced pressures from 0.005 to 0.78, and both single-channels and multi-channel heat sinks. Formulation of pressure

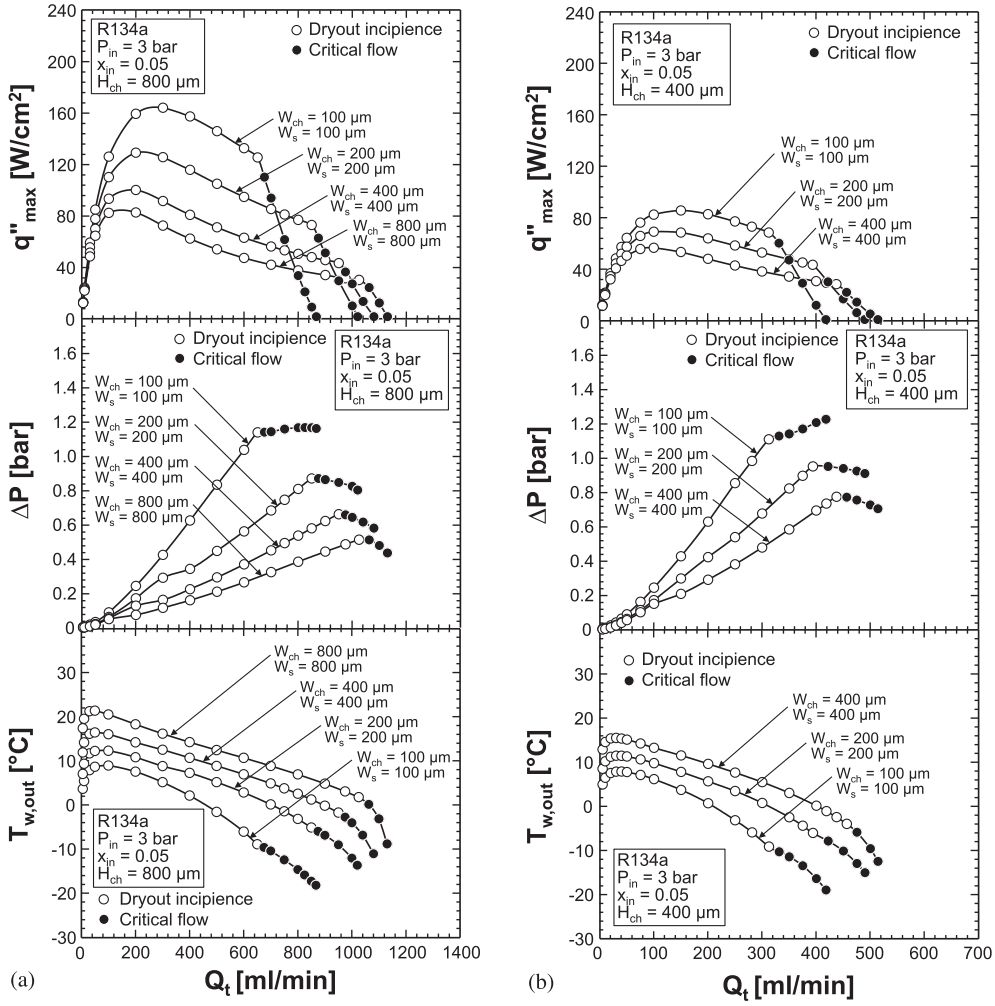

Fig. 4. Variations of maximum base heat flux and corresponding values of total pressure drop and bottom wall temperature at channel exit with total volume flow rate for different channel widths and sidewall thicknesses using R134a as working fluid: (a) H_{ch} = 800 μm and (b) H_{ch} = 400 μm.

drop in this correlation is based on the Lockhart-Martinelli separated flow model [41], where the two-phase frictional pressure gradient is expressed as the product of the frictional pressure gradient for the liquid phase and a two-phase pressure drop multiplier.

$$\left(\frac{dP}{dz}\right)_F = \left(\frac{dP}{dz}\right)_f \phi_f^2, \tag{9}$$

$$\text{where} \quad \phi_f^2 = 1 + \frac{C}{X} + \frac{1}{X^2}, \tag{10}$$

and X is the Lockhart–Martinelli parameter, which is the ratio of frictional pressure gradient for liquid to that for vapor, based on actual flow rates of the individual phases.

$$X^2 = \frac{(dP/dz)_f}{(dP/dz)_g}, \tag{11}$$

$$\text{where} \quad -\left(\frac{dP}{dz}\right)_f = \frac{2f_f v_f G^2 (1-x)^2}{D_h} \tag{12a}$$

$$\text{and} \quad -\left(\frac{dP}{dz}\right)_g = \frac{2f_g v_g G^2 x^2}{D_h}. \tag{12b}$$

The friction factor for phase k ($k = f$ for liquid or g for vapor) in Eqs. (12a) and (12b) is given by

$$f_k = 16\, Re_k^{-1} \quad \text{for } Re_k < 2000, \tag{13a}$$

$$f_k = 0.079\, Re_k^{-0.25} \quad \text{for } 2000 \leqslant Re_k < 20,000, \tag{13b}$$

$$\text{and} \quad f_k = 0.046\, Re_k^{-0.2} \quad \text{for } Re_k \geqslant 20,000, \tag{13c}$$

$$\text{where} \quad Re_k = Re_f = \frac{G(1-x)D_h}{\mu_f} \text{ for liquid,} \tag{14a}$$

$$\text{and} \quad Re_k = Re_g = \frac{GxD_h}{\mu_g} \text{for vapor.} \tag{14b}$$

For laminar flow in a rectangular channel, the two-phase friction factor can be expressed as a function of the channel's aspect ratio [67],

$$f_k Re_k = 24\left(1 - 1.3553\beta + 1.9467\beta^2 - 1.7012\beta^3 + 0.9564\beta^4 - 0.2537\beta^5\right). \tag{15}$$

For flow boiling in micro-channels, the function C in Eq. (10) for the two-phase pressure drop multiplier is calculated using

$$C = C_{non-boiling}\left[1 + 60We_{fo}^{0.32}\left(Bo\frac{P_H}{P_F}\right)^{0.78}\right] \quad \text{for } Re_f \geqslant 2000 \tag{16a}$$

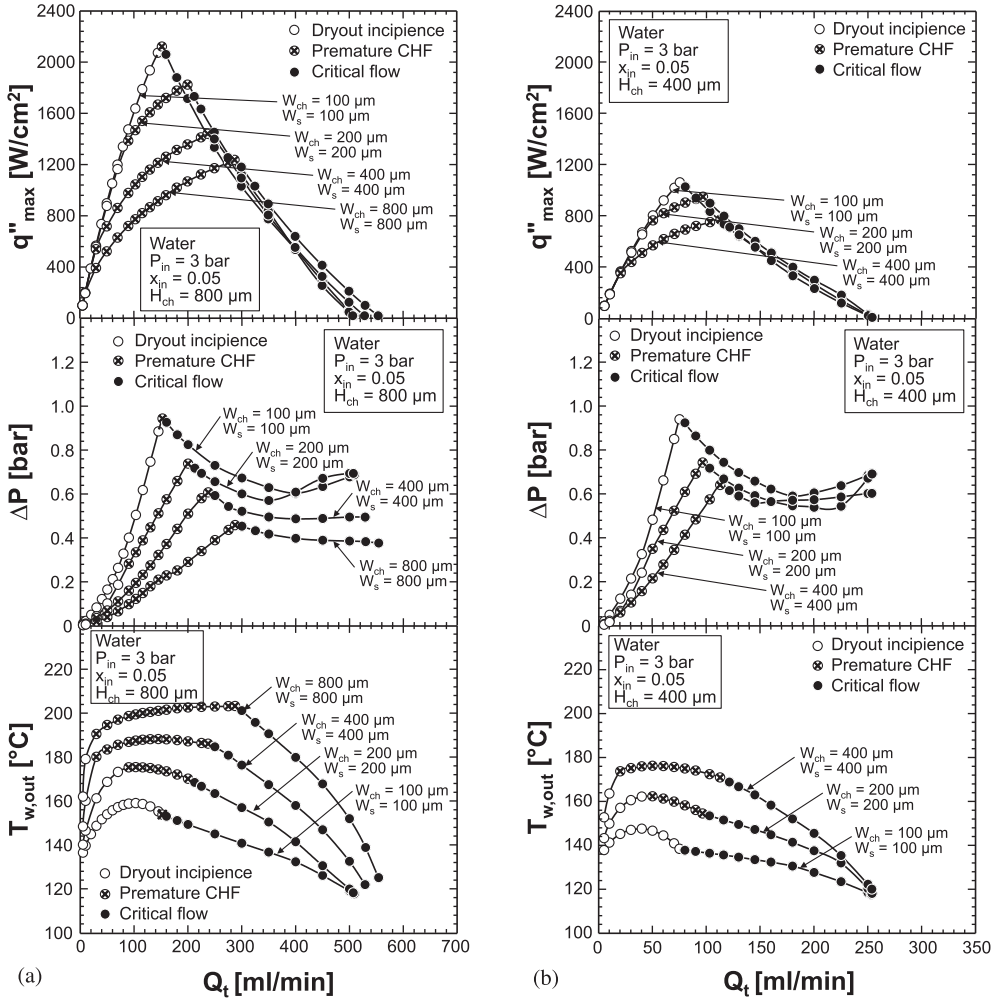

Fig. 5. Variations of maximum base heat flux and corresponding values of total pressure drop and bottom wall temperature at channel exit with total volume flow rate for different channel widths and sidewall thicknesses using water as working fluid: (a) H_{ch} = 800 μm and (b) H_{ch} = 400 μm.

and $$C = C_{non-boiling}\left[1 + 530We_{fo}^{0.52}\left(Bo\frac{P_H}{P_F}\right)^{1.09}\right] \quad \text{for } Re_f < 2000, \tag{16b}$$

where P_H/P_F is the ratio of the flow channel's heated to wetted perimeters, given by $P_H/P_F = (W_{ch} + 2H_{ch})/(2W_{ch} + 2H_{ch})$ for three-sided heating as shown in Fig. 2. In Eqs. (16a) and (16b), the liquid-only Weber number is defined as

$$We_{fo} = \frac{G^2 D_h}{\rho_f \sigma}, \tag{17}$$

and Boiling number expressed in terms of q''_H, the effective heat flux averaged over the heated perimeter of the channel,

$$Bo = \frac{q''_H}{Gh_{fg}}. \tag{18}$$

Also in Eqs. (16a) and (16b), the function $C_{non-boiling}$ was derived by the authors for non-boiling (adiabatic and condensing) flows [68] for different combinations of liquid and vapor states according to

$$C_{non-boiling} = 0.39Re_{fo}^{0.03}Su_{go}^{0.10}\left(\frac{\rho_f}{\rho_g}\right)^{0.35} \quad \text{for } Re_f \geqslant 2000,$$
$$Re_g \geqslant 2000 (tt), \tag{19a}$$

$$C_{non-boiling} = 8.7 \times 10^{-4}Re_{fo}^{0.17}Su_{go}^{0.50}\left(\frac{\rho_f}{\rho_g}\right)^{0.14} \quad \text{for } Re_f \geqslant 2000,$$
$$Re_g < 2000 (tv), \tag{19b}$$

$$C_{non-boiling} = 0.0015Re_{fo}^{0.59}Su_{go}^{0.19}\left(\frac{\rho_f}{\rho_g}\right)^{0.36} \quad \text{for } Re_f < 2000,$$
$$Re_g \geqslant 2000 (vt), \tag{19c}$$

and $$C_{non-boiling} = 3.5 \times 10^{-5}Re_{fo}^{0.44}Su_{go}^{0.50}\left(\frac{\rho_f}{\rho_g}\right)^{0.48}$$
$$\text{for } Re_f < 2000,\ Re_g < 2000 (vv). \tag{19d}$$

The two-phase pressure drop is determined by integrating the relations for accelerational and frictional pressure gradients numerically according to

$$\Delta P_{tp} = \int_0^{L_{tp}} \left[-\left(\frac{dP}{dz}\right)_A - \left(\frac{dP}{dz}\right)_F\right] dz. \tag{20}$$

In this study, local saturation temperature as well as thermophysical properties of liquid and vapor are based on local saturation pressure. Thermophysical properties for R134a and water are obtained using REFPROP 8.0 software from NIST [69], and those for HFE-7100 from 3 M Company.

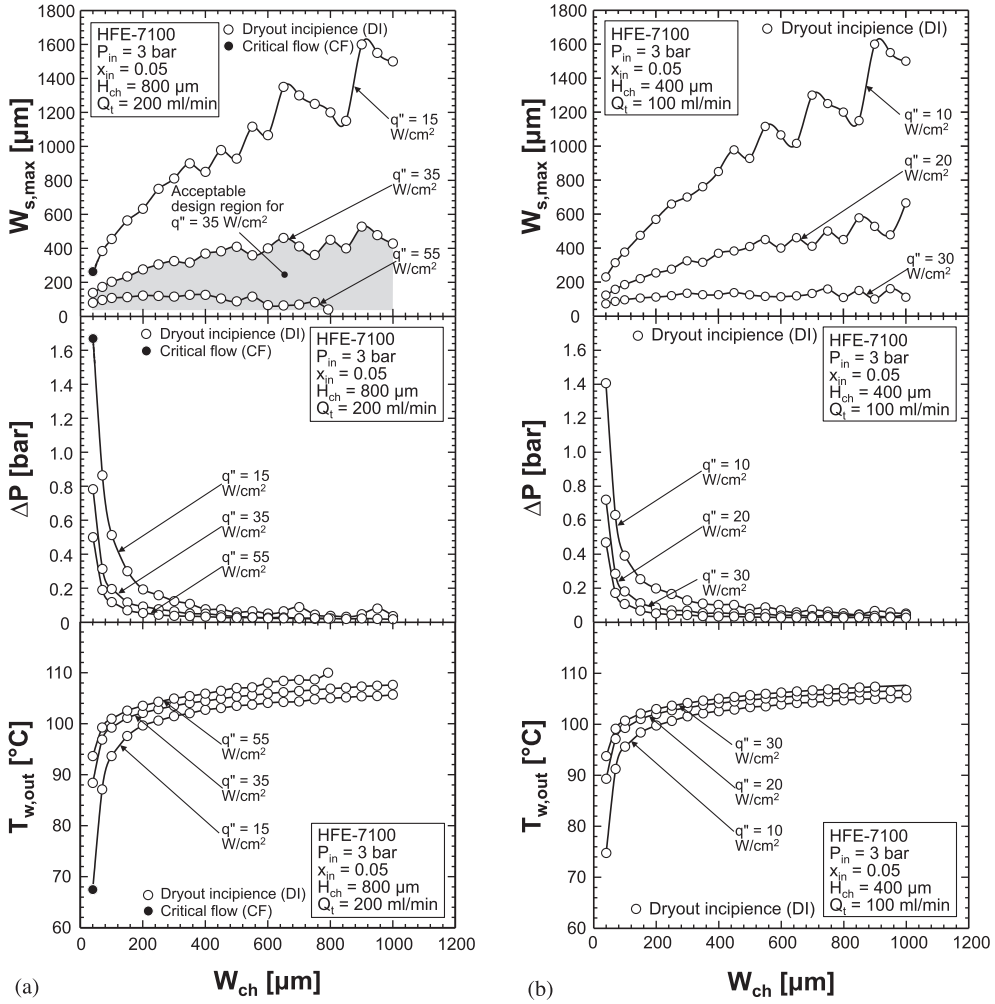

Fig. 6. Variations of maximum sidewall width and corresponding values of total pressure drop and bottom wall temperature at channel exit with channel width for different base heat fluxes using HFE-7100 as working fluid: (a) H_{ch} = 800 μm and (b) H_{ch} = 400 μm.

2.3. Heat transfer in micro-channels

For a rectangular micro-channel heat sink with three-sided heating (*i.e.*, with a perfectly insulating top cover plate), applying the fin analysis method to the micro-channel unit cell shown in Fig. 2 yields the following relation for temperature along the plane of the micro-channel's bottom wall,

$$T_w = \frac{q''(W_{ch}+W_s)}{h_{tp}(W_{ch}+2\eta H_{ch})} + T_{sat} = \frac{q''(W_{ch}+2H_{ch})}{h_{tp}(W_{ch}+2\eta H_{ch})} + T_{sat}, \tag{21}$$

where the fin efficiency and fin parameter are defined, respectively, as [70]

$$\eta = \frac{\tanh(mH_{ch})}{mH_{ch}} \tag{22a}$$

and $$m = \sqrt{2h_{tp}/(kW_s)}. \tag{22b}$$

The saturated flow boiling heat transfer coefficient is determined using the authors' universal heat transfer correlation for saturated flow boiling in mini/micro-channels [61]. This correlation is based on a consolidated database consisting of 10,805 pre-dryout data points amassed from 31 sources, which consists of 18 working fluids, hydraulic diameters of 0.19–6.5 mm, mass velocities of 19–1608 kg/m^2 s, liquid-only Reynolds numbers of 57–49,820, qualities of 0–1, and reduced pressures of 0.005–0.69. The correlation is constructed by superpositioning the contributions of nucleate boiling and convective boiling according to

$$h_{tp} = \left(h_{nb}^2 + h_{cb}^2\right)^{0.5}, \tag{23}$$

where $$h_{nb} = \left[2345\left(Bo\frac{P_H}{P_F}\right)^{0.70} P_R^{0.38}(1-x)^{-0.51}\right]\left(0.023\mathrm{Re}_f^{0.8}\mathrm{Pr}_f^{0.4}\frac{k_f}{D_h}\right) \tag{24a}$$

and $$h_{cb} = \left[5.2\left(Bo\frac{P_H}{P_F}\right)^{0.08} We_{fo}^{-0.54} + 3.5\left(\frac{1}{X_{tt}}\right)^{0.94}\left(\frac{\rho_g}{\rho_f}\right)^{0.25}\right] \times \left(0.023\mathrm{Re}_f^{0.8}\mathrm{Pr}_f^{0.4}\frac{k_f}{D_h}\right). \tag{24b}$$

The reduced pressure, P_R, in Eq. (24a) and Lockhart-Martinelli parameter, X_{tt}, in Eq. (24b) are defined, respectively, as

$$P_R = \frac{P}{P_{crit}} \tag{25}$$

and $$X_{tt} = \left(\frac{\mu_f}{\mu_g}\right)^{0.1}\left(\frac{1-x}{x}\right)^{0.9}\left(\frac{\rho_g}{\rho_f}\right)^{0.5}. \tag{26}$$

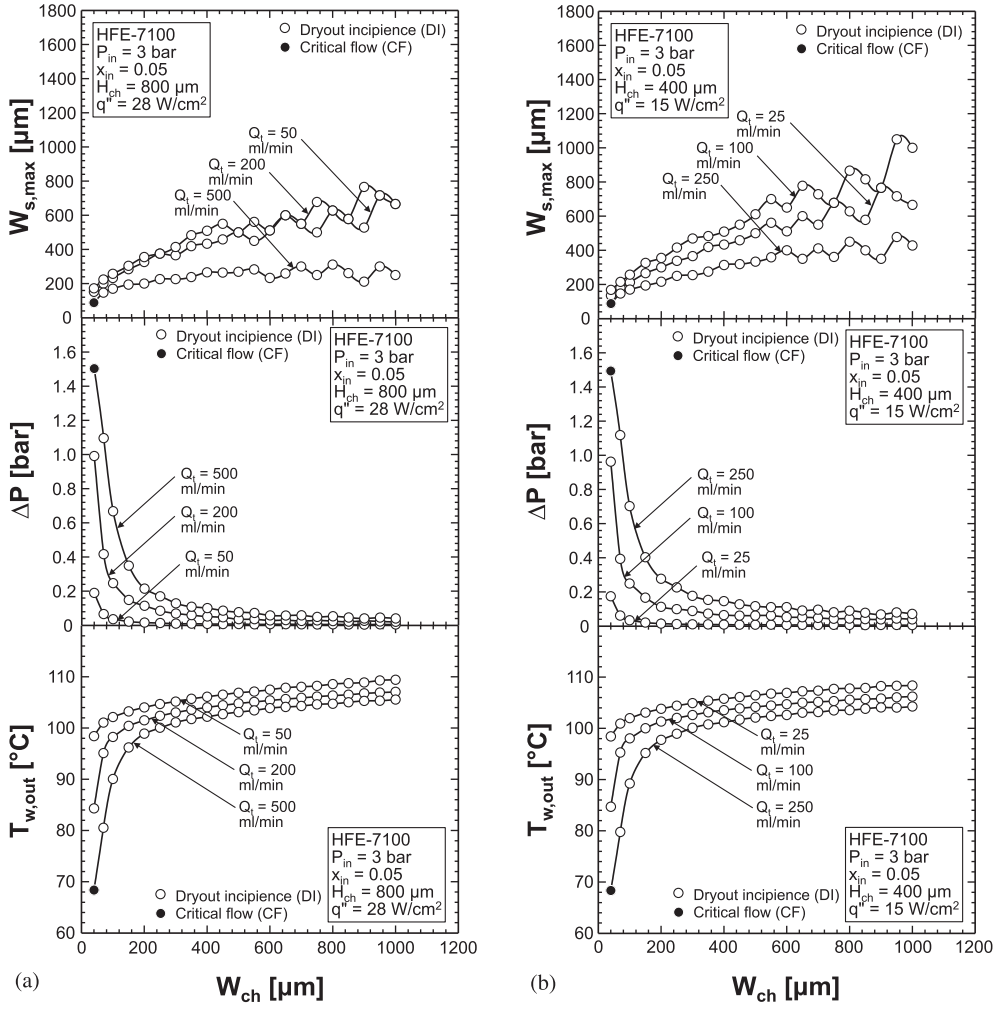

Fig. 7. Variations of maximum sidewall width and corresponding values of total pressure drop and bottom wall temperature at channel exit with channel width for different total volume flow rates using HFE-7100 as working fluid: (a) H_{ch} = 800 μm and (b) H_{ch} = 400 μm.

2.4. Heat transfer and flow limits

2.4.1. Dryout incipience

CHF is arguably the most important thermal design parameter for micro-channel heat sinks intended for cooling heat-flux controlled devices, and exceeding this limit can lead to catastrophic device failure due to overheating. As discussed earlier, CHF in micro-channels is triggered mostly by complete dryout of the annular liquid film. An important precursor to this event is dryout incipience, corresponding to localized dryout of the annular film, which occurs upstream of the point of complete dryout. Dryout incipience therefore serves as a very effective thermal design limit for heat flux, including a safety margin. The quality x_{di} corresponding to dryout incipience is determined from the authors' recent universal correlation [60] consisting of 997 data points from 26 source, which consists of 13 working fluids, hydraulic diameters from 0.51 to 6.0 mm, mass velocities from 29 to 2303 kg/m^2 s, liquid-only Reynolds numbers from 125 to 53,770, Boiling numbers from 0.31×10^{-4} to 44.3×10^{-4}, and reduced pressures from 0.005 to 0.78. The dryout incipience quality is given by

$$x_{di} = 1.4We_{fo}^{0.03}P_R^{0.08} - 15.0\left(Bo\frac{P_H}{P_F}\right)^{0.15}Ca^{0.35}\left(\frac{\rho_g}{\rho_f}\right)^{0.06}, \quad (27)$$

where Ca is the capillary number, defined as

$$Ca = \frac{\mu_f G}{\rho_f \sigma}. \quad (28)$$

2.4.2. Premature critical heat flux

As discussed earlier, premature CHF is associated with appreciable flow reseveral and instabilities. In the present study, it is calculated using the premature CHF correlation by Qu and Mudawar [62]. This correlation is based on water data for a micro-channel heat sink with D_h = 341 μm and three-sided wall heating, and R113 data for two separate heat sinks, one containing circular mini-channels with D = 2.54 mm, and the other circular micro-channels with D = 0.51 mm. This correlation allows the prediction of heat flux corresponding to premature CHF averaged over the heated perimeter of channel,

$$q''_{P-CHF} = 33.43Gh_{fg}\left(\frac{\rho_g}{\rho_f}\right)^{1.11}We_L^{-0.21}\left(\frac{L}{D_h}\right)^{-0.36}, \quad (29)$$

where We_L is Weber number based on the channel's heated length, defined as

$$We_L = \frac{G^2 L}{\rho_f \sigma}. \quad (30)$$

2.4.3. Two-phase critical flow (two-phase choking)

In a previous study by the authors [58] addressing the relationship between two-phase critical flow, premature CHF, and CHF in

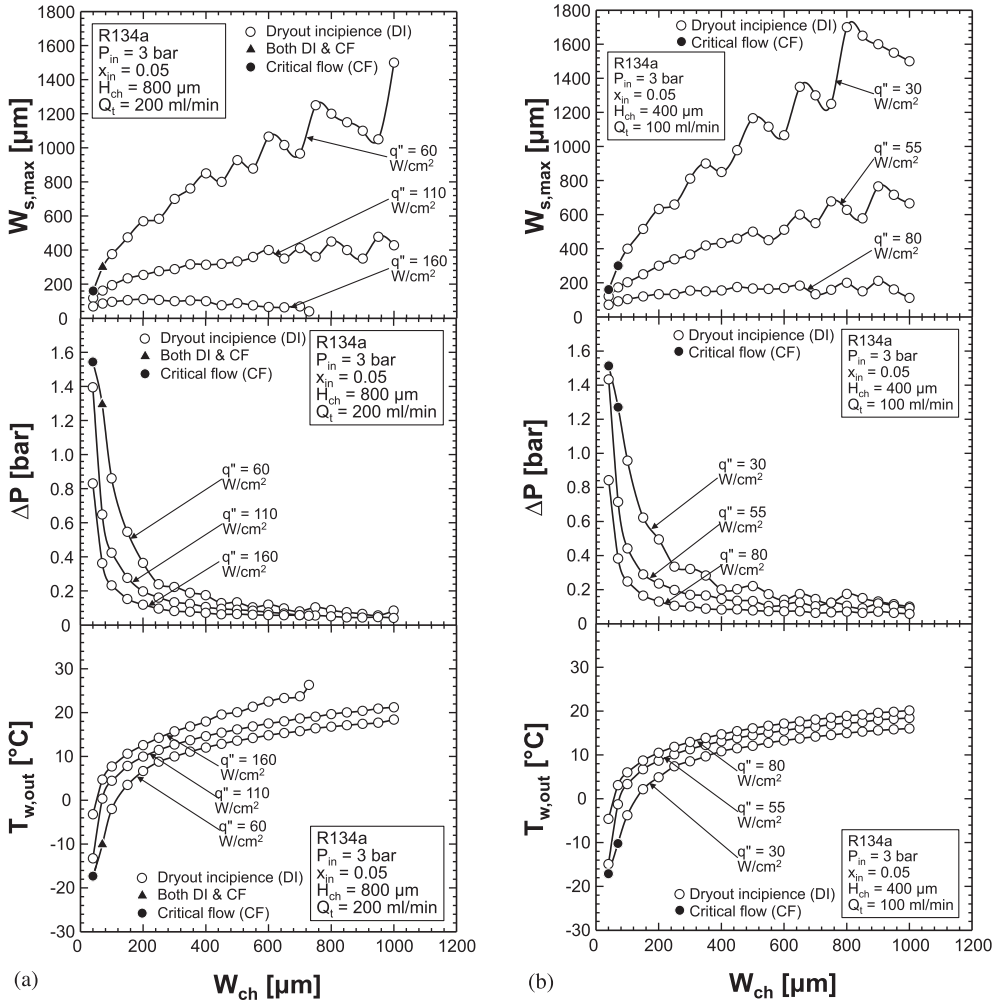

Fig. 8. Variations of maximum sidewall width and corresponding values of total pressure drop and bottom wall temperature at channel exit with channel width for different base heat fluxes using R134a as working fluid: (a) H_{ch} = 800 μm and (b) H_{ch} = 400 μm.

micro-channel heat sinks, the Homogeneous Frozen Model (HFM) derived by Wallis [71] for homogeneous flow with negligible flashing, showed the most superior predictions of experimental critical flow data. In the present study study, the HFM is used to predict mass velocity corresponding to critical flow (also commonly referred to as two-phase choked flow) according to

$$G_c = \left\{ -\left[x\frac{dv_g}{dP} + (1-x)\frac{dv_f}{dP} \right] \right\}^{-0.5}. \tag{31}$$

2.5. Overall calculation methodology

Summarized in Table 3 are key predictive methods used in the present study along with the applicable range of channel diameter and working fluids. Notice that the correlations for frictional pressure gradient [59], saturated flow boiling heat transfer [61], and dryout incipience [62] are generalized universal predictive tools intended specifically for mini/micro-channels and applicable to very broad ranges of operating parameters and many working fluids. Using a finite difference scheme, relevant equations are solved numerically by dividing the channel length into small Δz increments and marching forward starting with known micro-channel inlet conditions. Local values of x_{di} and G_c are calculated at every node along the micro-channel based on local thermophysical properties using Eqs. (27) and (31), respectively. Occurrence of dryout incipience or two-phase critical flow is checked by comparing local values of x and x_{di}, and G and G_c, respectively, at each node. The occurrence of premature CHF is determined by comparing q''_H and q''_{P-CHF}, where thermophysical properties are based on the channel's outlet pressure.

3. Thermal design of micro-channel heat sinks for HFE-7100, R134a, and water

3.1. Maximum heat flux and corresponding pressure drop and wall temperature

Figs. 3–5 show variations of maximum base heat flux, q''_{max}, and corresponding values of total pressure drop, ΔP, and bottom wall temperature at channel exit, $T_{w,out}$, (heat sink's highest bottom wall temperature) with total volume flow rate, Q_t, for different channel widths and sidewall thicknesses using HFE-7100, R134a, and water, respectively, as working fluids. As discussed earlier, cooling performance of the micro-channel heat sink is governed by two heat transfer limits, dryout incipience and premature CHF, and one flow limit, two-phase critical flow. Only one of the three limits will be dominant for a given combination of H_{ch}, W_{ch}, W_s, and Q_t, and the dominant limit is therefore used to determine q''_{max}.

For HFE-7100, Fig. 3(a) and (b), and R134a, Fig. 4(a) and (b), q''_{max} is limited by dryout incipience for low Q_t, and two-phase critical

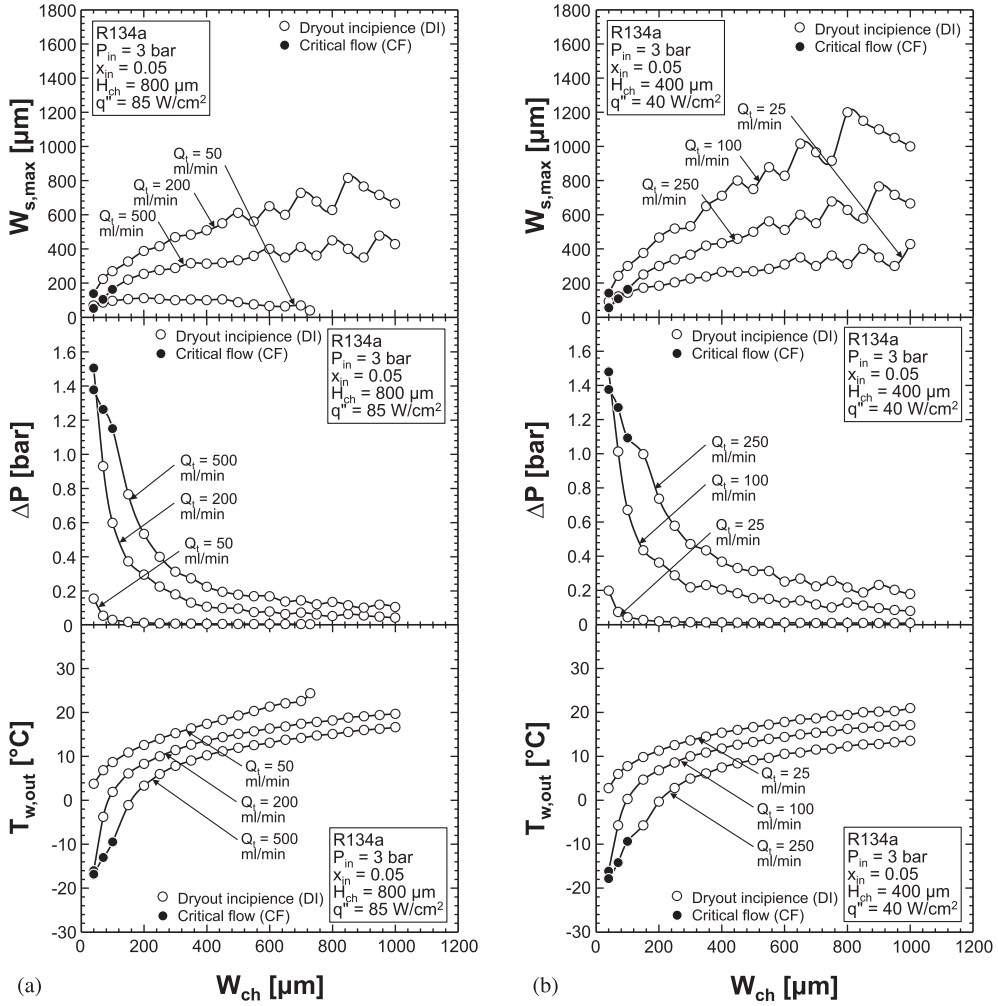

Fig. 9. Variations of maximum width of sidewall width and corresponding values of total pressure drop and bottom wall temperature at channel exit with channel width for different total volume flow rates using R134a as working fluid: (a) H_{ch} = 800 μm and (b) H_{ch} = 400 μm.

flow for high Q_t. As Q_t is increased within the dryout incipience dominant region, q''_{max} increases at a steep rate up to a certain point then decreases gradually. Within the critical flow dominant region, q''_{max} decreases very sharply. Notice that, for a given fluid and prescribed set of operating conditions, the acceptable design range for safe heat sink operation is confined to the region below the line corresponding to q''_{max}, which is depicted by the gray area in Fig. 3(a) corresponding to HFE-7100 with P_{in} = 3 bar, x_{in} = 0.05, H_{ch} = 800 μm, and $W_{ch} = W_s$ = 100 μm. Notice in Figs. 3 (a), (b) and 4(a), (b) how smaller values of W_{ch} and W_s increase q''_{max} but promote transition to the critical flow dominant region at a smaller Q_t. This is further confirmation that smaller hydraulic diameter is advantageous to micro-channel cooling.

As shown in Fig. 3(a) and (b) for HFE-7100, and 4(a) and 4(b) for R134a, ΔP calculated by setting $q'' = q''_{max}$ increases monotonically with increasing Q_t within the dryout incipience dominant region but generally decreases in the critical flow dominant region. Excepting very low Q_t values, $T_{w,out}$ calculated by setting $q'' = q''_{max}$ decreases monotonically with increasing Q_t within both the dryout incipience and critical flow dominant regions. Figs. 3(a), (b) and 4 (a), (b) clearly show the cooling advantage of decreasing W_{ch} and W_s by decreasing $T_{w,out}$. However, the advantage of smaller hydraulic diameter is realized with a higher ΔP penalty.

Fig. 5(a) and (b) shows that, unlike HFE-7100 and R134a, where q''_{max} is limited by either dryout incipience or critical flow, q''_{max} for water can also be limited by premature CHF, which is smaller than q''_{max} corresponding to dryout incipience. Decreasing W_{ch} and W_s increases q''_{max} for both the dryout incipience and premature CHF dominant regions corresponding to lower Q_t values, but the influence W_{ch} and W_s on q''_{max} is minimal at high Q_t. Similar to HFE-7100 and R134a, decreasing W_{ch} and W_s provides better cooling for water, evidenced by lower $T_{w,out}$, and this is advantage is realized with a larger pressure drop penalty.

For all three fluids, the larger channel height of H_{ch} = 800 μm (*i.e.*, deeper micro-channels), Figs. 3(a), 4(a), and 5(a), yields appreciable enhancement in cooling performance, nearly doubling peak q''_{max} compared to H_{ch} = 400 μm, Figs. 3(b), 4 (b), and 5(b), while producing a relatively weak adverse effect on $T_{w,out}$. Another advantage of the deeper micro-channel is greatly decreasing ΔP.

Overall, q''_{max} for water is far greater than for both HFE-7100 and R134a without suffering appreciable pressure drop, while R134a achieves lower $T_{w,out}$ compared to both HFE-7100 and water.

The trends of q''_{max} and corresponding ΔP and $T_{w,out}$ provide important guidelines when addressing different aspects of micro-channel performance, namely, upper flux limit, pumping power penalty, and cooling effectiveness. Overall, this design methodology allows a cooling system designer to achieve the best compromise when selecting optimum ranges of heat sink geometrical parameters and operating condition, in terms of safely dissipating the heat, maintaining device temperature below an acceptable limit, and minimizing pumping power.

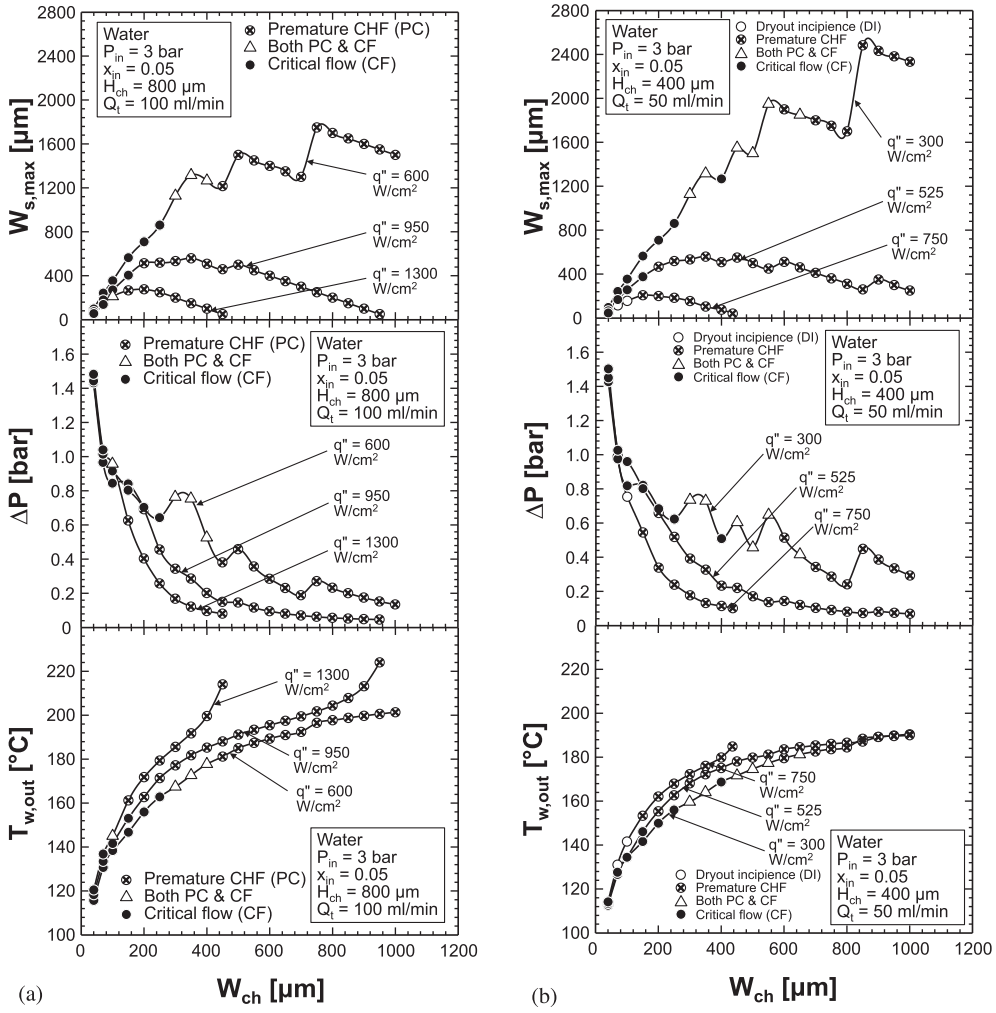

Fig. 10. Variations of maximum sidewall width and corresponding values of total pressure drop and bottom wall temperature at channel exit with channel width for different base heat fluxes using water as working fluid: (a) H_{ch} = 800 μm and (b) H_{ch} = 400 μm.

3.2. Maximum sidewall width and corresponding pressure drop and wall temperature

The results discussed above are for sidewall thickness equal to channel width, $W_s = W_{ch}$. However, sidewall thickness represents another independent parameter that has a significant influence on pressure drop and thermal design. For fixed W_{ch}, Eq. (1) shows that increasing W_s decreases the number of micro-channels, N, in the heat sink, therefore increasing mass velocity, G. Therefore, the highest G is achieved when sidewall thickness is equal to $W_{s,max}$. Fig. 6(a) and (b) show, for HFE-7100, variations of maximum sidewall width, $W_{s,max}$, and corresponding values of ΔP and $T_{w,out}$ (calculated by setting $W_s = W_{s,max}$) with W_{ch} for different values of q''; Fig. 7(a) and (b) show variations of $W_{s,max}$ for different values of Q_t. Similar plots are shown for R134a in Figs. 8(a), (b) and 9(a), (b) and for water in Figs. 10(a), (b) and 11(a), (b).

For HFE-7100 and R134a, $W_{s,max}$ is limited mostly by dryout incipience for most W_{ch} values, and by critical flow for very small W_{ch}. For water, $W_{s,max}$ is limited mostly by two-phase critical flow for small W_{ch} values, and premature CHF for larger W_{ch} values. However, as shown in Fig. 11(a) and (b), $W_{s,max}$ for high Q_t is limited by critical flow over the entire range of W_{ch}.

As shown in Figs. 6(a), (b), and 7(a), (b) for HFE-7100, Figs. 8(a), (b), and 9(a), (b) for R134a, and Figs. 10(a), (b), and 11(a), (b) for water, $W_{s,max}$ generally increases with increasing W_{ch}. However, there are some exceptions to this trend, which include higher q'' cases for HFE-7100, Fig. 6(a), R134a, Fig. 8(a), and water, Fig. 10 (a) and (b), where $W_{s,max}$ increases to a maximum then decreases to the minimum value of 40 μm corresponding to the W_s constraint given in Table 1. A similar trend is observed for lower Q_t cases for R134a, Fig. 9(a), and water, Fig. 11(a) and (b). Notice that the fluctuations in parametric trends of $W_{s,max}$, especially for high W_{ch} values, are associated with the smaller number of channels in the heat sink causing appreciable changes in $W_{s,max}$ value with respect to W_{ch}. The acceptable design range is limited by the region below the line corresponding to $W_{s,max}$ for a given set of operating conditions. This is represented by the gray area in Fig. 6(a) for HFE-7100 with H_{ch} = 800 μm and q'' = 35 W/cm^2.

Figs. 6(a), (b), and 7(a), (b) for HFE-7100, Figs. 8(a), (b), and 9 (a), (b) for R134a, and Figs. 10(a), (b), and 11(a), (b) for water, all show increasing W_{ch} causes a decrease in ΔP coupled with an increase in $T_{w,out}$ corresponding to $W_{s,max}$. These trends are the result of the increase in W_{ch} decreasing the number of micro-channels, N, which also decreases mass velocity, G, in the micro-channels. Notice in the same figures how two-phase critical flow is encountered at smaller values of W_{ch}, where ΔP is highest and $T_{w,out}$ lowest.

Fig. 6(a) and (b) for HFE-7100, Fig. 8(a) and (b) for R134a, and Fig. 10(a) and (b) for water show the influence of q'' on $W_{s,max}$ for fixed Q_t values corresponding to the highest q''_{max} value from

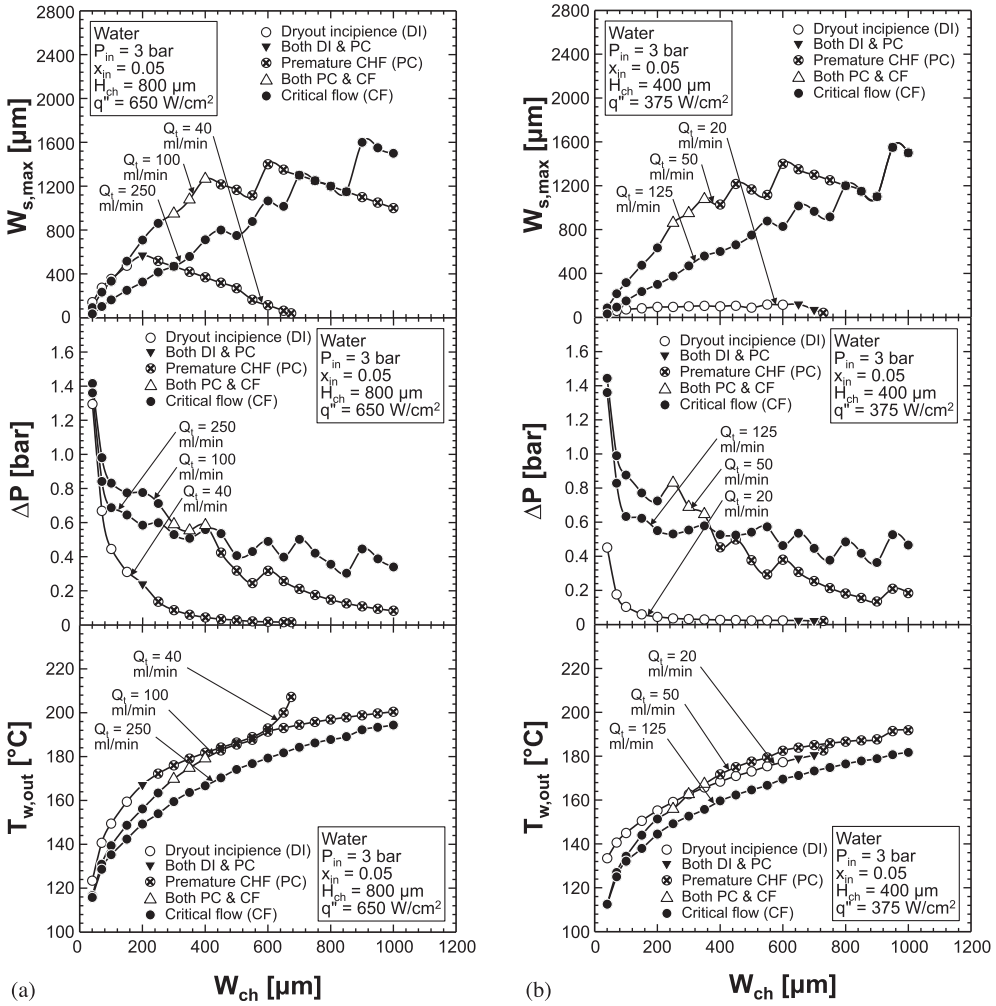

Fig. 11. Variations of maximum sidewall width and corresponding values of total pressure drop and bottom wall temperature at channel exit with channel width for different total volume flow rates using water as working fluid: (a) H_{ch} = 800 μm and (b) H_{ch} = 400 μm.

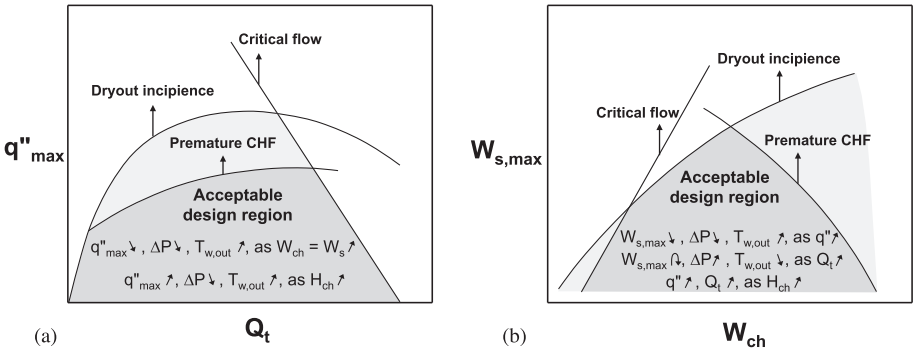

Fig. 12. Qualitative representation of acceptable design regions for saturated flow boiling in micro-channel heat sinks for (a) maximum heat flux and (b) maximum sidewall thickness. The premature CHF limit in both plots is specific to water.

Fig. 3(a) and (b) for HFE-7100, Fig. 4(a) and (b) for R134a, and Fig. 5 (a) and (b) for water, respectively. These figures show $W_{s,\max}$ decreases with increasing q'', which, for fixed W_{ch} and Q_t, increases N and decreases G, resulting in smaller ΔP and higher $T_{w,out}$.

Fig. 7(a) and (b) for HFE-7100, Fig. 9(a) and (b) for R134a, and Fig. 11(a) and (b) for water show the influence of Q_t on $W_{s,\max}$ for fixed q''. The q'' value in Fig. 7(a) and (b) for HFE-7100 is approximately half the highest $q''_{\max}$ value in Figs. 3(a) and (b), respectively. Similarly, the q'' value in Fig. 9(a) and (b) for R134a is approximately half of highest $q''_{\max}$ value in Fig. 4(a) and (b), respectively. For water, the q'' value in Fig. 11(a) and (b) is approximately one-third the highest $q''_{\max}$ value in Fig. 5(a) and (b), respectively. These figures show that the variation of $W_{s,\max}$ with respect to Q_t is not monotonic; $W_{s,\max}$ increases initially with increasing Q_t then decreases.

Overall, the $W_{s,\max}$ plots for the three fluids show that, for fixed W_{ch} and W_s, the larger H_{ch} (*i.e.*, deeper micro-channels) allows for much higher q'' corresponding to relatively small changes in ΔP

and $T_{w,out}$. The larger H_{ch} also facilitates increasing Q_t corresponding to small changes in ΔP and $T_{w,out}$.

The parametric trends for q''_{max} and $W_{s,max}$ are qualitatively summarized in Fig. 12(a) and (b), respectively. In general, micro-channels with smaller W_{ch} and W_s increase q''_{max}, and $W_{s,max}$ decreases with increasing q''. Additionally, increasing H_{ch} allows for much higher q'' corresponding to relatively small changes in ΔP and $T_{w,out}$. Increasing H_{ch} also facilitates increasing Q_t corresponding to small changes in ΔP and $T_{w,out}$. These figures also illustrate important flow and heat transfer limits encountered in micro-channel heat sinks, and the acceptable design region circumscribed by these limits. Fig. 12(a) shows q''_{max} is limited by dryout incipience at low Q_t, and two-phase critical flow at high Q_t. For water, premature CHF is an important limit that falls below the dryout incipience limit. Fig. 12(b) shows $W_{s,max}$ is limited by two-phase critical flow, dryout incipience, and premature CHF, with critical flow generally occurring at smaller W_{ch} values, and premature CHF at larger W_{ch} values, especially for water.

3.3. Future research needs

It is important to emphasize that the accuracy of models and correlations employed in the present study are entirely dependent on availability of databases, especially those employing advanced diagnostic methods to capture interfacial behavior for different fluids and broad ranges of operating conditions. Overall, more data are needed to improve predictive relations for both premature CHF and critical flow. Detailed discussions of advanced diagnostic methods for measurement of temperature, interfacial velocity, and liquid velocity in two-phase flows are available in [72–75], [74–77], and [76–78], respectively.

4. Conclusions

This study provided a comprehensive methodology for thermal design of micro-channel heat sinks with saturated inlet conditions. Predictive methods for pressure drop and heat transfer were summarized. Also presented were thermal limits associated with dryout incipience and premature critical heat flux, as well as two-phase critical flow limit. The three limits were combined to define an envelope for acceptable heat sink performance. Special emphasis was placed on utilizing universal correlations that rely on large databases amassed from numerous sources, and which encompass many working fluids, and very broad ranges of hydraulic diameter, mass velocity, inlet pressure, and inlet quality. Key findings from the study are as follows:

1. A parametric study was performed to determine the variation of maximum heat flux, q''_{max}, with total volumetric flow rate, Q_t, for different combinations of channel geometrical parameters (W_{ch}, W_s, H_{ch}) for three working fluids, HFE-7100, R134a, and water. Then q''_{max} values were used to assess corresponding variations of pressure drop, ΔP, and maximum bottom wall temperature, $T_{w,out}$. For both HFE-7100 and R134a, the parametric study shows q''_{max} is limited by dryout incipience for low Q_t, and two-phase critical flow for high Q_t. For water, q''_{max} is also limited by premature CHF for intermediate values of Q_t. For fixed Q_t, q''_{max} can be increased significantly, and $T_{w,out}$ decreased by decreasing W_{ch} and W_s (*i.e.*, by using a larger number of smaller channels), albeit at the expense of higher ΔP. Increasing H_{ch} (*i.e.*, using deeper micro-channels) serves to increase q''_{max} and decrease ΔP, while producing a relatively weak adverse effect on $T_{w,out}$.
2. For HFE-7100 and R134a, $W_{s,max}$ is limited mostly by dryout incipience for most W_{ch} values, and by critical flow for very small W_{ch}. For water, $W_{s,max}$ is limited mostly by two-phase critical flow for small W_{ch} values, and premature CHF for larger W_{ch} values. Increasing W_{ch} causes a decrease in ΔP coupled with an increase in $T_{w,out}$ corresponding to $W_{s,max}$. These trends are the result of the increase in W_{ch} decreasing the number of micro-channels, which also decreases mass velocity, G, in the micro-channels.
3. Despite the specific fluids and limits examined, this study provides a systematic methodology the reader may follow to address other fluids or operating conditions of interest. The trends of q''_{max} and corresponding trends of ΔP and $T_{w,out}$ provide an effective means for achieving the best compromise when selecting optimum ranges of heat sink geometrical parameters and operating conditions, in terms of safely dissipating the heat, maintaining acceptable device temperature, and minimizing pumping power.

Acknowledgements

This work was supported by the National Research Foundation of Korea (NRF) grant funded by the Korea government (MSIP) (No. NRF-2015R1C1A1A01055439), and by the National Aeronautics and Space Administration (NASA) (Grant No. NNX13AB01G).

References

[1] I. Mudawar, Assessment of high-heat-flux thermal management schemes, IEEE Trans. CPMT: Compon. Packag. Technol. 24 (2001) 122–141.
[2] P.J. Marto, V.J. Lepere, Pool boiling heat transfer from enhanced surfaces to dielectric fluids, J. Heat Transfer – Trans. ASME 104 (1982) 292–299.
[3] I. Mudawar, T.M. Anderson, Parametric investigation into the effects of pressure, subcooling, surface augmentation and choice of coolant on pool boiling in the design of cooling systems for high-power density chips, J. Electron. Packag. – Trans. ASME 112 (1990) 375–382.
[4] A. Niro, G.P. Beretta, Boiling regimes in a closed two-phase thermosyphon, Int. J. Heat Mass Transfer 33 (1990) 2099–2110.
[5] I. Mudawar, T.M. Anderson, Optimization of extended surfaces for high flux chip cooling by pool boiling, J. Electron. Packag. – Trans. ASME 115 (1993) 89–100.
[6] I.L. Pioro, W. Rohsenow, S.S. Doerffer, Nucleate pool-boiling heat transfer. I: review of parametric effects of boiling surface, Int. J. Heat Mass Transfer 47 (2004) 5033–5044.
[7] I. Mudawar, Recent advances in high-flux, two-phase thermal management, J. Therm. Sci. Eng. Appl. – Trans. ASME 5 (2013) 021012.
[8] M. Monde, Y. Katto, Burnout in high heat-flux boiling system with an impinging jet, Int. J. Heat Mass Transfer 21 (1978) 295–305.
[9] Y. Kato, M. Shimizu, Upper limit of CHF in the saturated forced convection boiling system with an impinging jet, J. Heat Transfer – Trans. ASME 101 (1979) 265–269.
[10] M. Monde, Critical heat flux in saturated forced convection boiling on a heated disk with an impinging jet, J. Heat Transfer – Trans. ASME 109 (1987) 991–996.
[11] M. Monde, T. Inoue, Critical heat flux in saturated forced convection boiling on a heated disk with multiple jets, J. Heat Transfer – Trans. ASME 113 (1991) 722–727.
[12] D.C. Wadsworth, I. Mudawar, Enhancement of single-phase heat transfer and critical heat flux from an ultra-high-flux-source to a rectangular impinging jet of dielectric liquid, J. Heat Transfer – Trans. ASME 114 (1992) 764–768.
[13] M.E. Johns, I. Mudawar, An ultra-high power two-phase jet-impingement avionic clamshell module, J. Electron. Packag. – Trans. ASME 118 (1996) 264–270.
[14] S. Toda, A study in mist cooling (1st report: investigation of mist cooling), Trans. JSME 38 (1972) 581–588.
[15] J.P. Holman, C.M. Kendall, Extended studies of spray cooling with Freon-113, Int. J. Heat Mass Transfer 36 (1993) 2239–2241.
[16] D.D. Hall, I. Mudawar, Experimental and numerical study of quenching complex-shaped metallic alloys with multiple, overlapping sprays, Int. J. Heat Mass Transfer 38 (1995) 1201–1216.
[17] L. Lin, R. Ponnappan, Heat transfer characteristics of spray cooling in a closed loop, Int. J. Heat Mass Transfer 46 (2003) 3737–3746.
[18] M. Visaria, I. Mudawar, Theoretical and experimental study of the effects of spray inclination on two-phase spray cooling and critical heat flux, Int. J. Heat Mass Transfer 51 (2008) 2398–2410.
[19] M. Visaria, I. Mudawar, Effects of high subcooling on two-phase spray cooling and critical heat flux, Int. J. Heat Mass Transfer 51 (2008) 5269–5278.
[20] I. Mudawar, D. Bharathan, K. Kelly, S. Narumanchi, Two-phase spray cooling of hybrid vehicle electronics, IEEE Trans. – CPMT: Compon. Packag. Technol. 32 (2009) 501–512.

[21] I. Mudawar, Two-phase micro-channel heat sinks: theory, applications and limitations, J. Electron. Packag. – Trans. ASME 133 (2011) 041002.
[22] S. Mukherjee, I. Mudawar, Smart pumpless loop for micro-channel electronic cooling using flat and enhanced surfaces, IEEE Trans. – CPMT: Compon. Packag. Technol. 26 (2003) 99–109.
[23] S. Mukherjee, I. Mudawar, Pumpless loop for narrow channel and micro-channel boiling from vertical surfaces, J. Electron. Packag. – Trans. ASME 125 (2003) 431–441.
[24] M.K. Sung, I. Mudawar, Experimental and numerical investigation of single-phase heat transfer using a hybrid jet-impingement/micro-channel cooling scheme, Int. J. Heat Mass Transfer 49 (2006) 682–694.
[25] S.M. Kim, I. Mudawar, Review of databases and predictive methods for pressure drop in adiabatic, condensing and boiling mini/micro-channel flows, Int. J. Heat Mass Transfer 77 (2014) 74–97.
[26] W.H. McAdams, W.K. Woods, L.C. Heroman, Vaporization inside horizontal tubes, II. Benzene-oil mixture, Trans. ASME 64 (1942) 193–200.
[27] W.W. Akers, H.A. Deans, O.K. Crosser, Condensing heat transfer within horizontal tubes, Chem. Eng. Prog. 54 (1958) 89–90.
[28] A. Cicchitti, C. Lombardi, M. Silvestri, G. Soldaini, R. Zavalluilli, Two-phase cooling experiments-pressure drop, heat transfer and burnout measurements, Energia Nucleare 7 (1960) 407–425.
[29] W.L. Owens, Two-phase pressure gradient, Int. Dev. Heat Transfer (Pt. II) (1991), ASME, New York.
[30] A.E. Dukler, M. Wicks, R.G. Cleaveland, Pressure drop and hold up in two-phase flow, AIChE J. 10 (1964) 38–51.
[31] D.R.H. Beattie, P.B. Whalley, A simple two-phase frictional pressure drop calculation method, Int. J. Multiphase Flow 8 (1982) 83–87.
[32] C.Y. Yang, R.L. Webb, Friction pressure drop of R-12 in small hydraulic diameter extruded aluminum tubes with and without micro-fins, Int. J. Heat Mass Transfer 39 (1996) 801–809.
[33] Y.Y. Yan, T.F. Lin, Evaporation heat transfer and pressure drop of refrigerant R-134a in a small pipe, Int. J. Heat Mass Transfer 41 (1998) 4183–4194.
[34] H.J. Lee, S.Y. Lee, Pressure drop correlations for two-phase flow within horizontal rectangular channels with small heights, Int. J. Multiphase Flow 27 (2001) 783–796.
[35] W. Yu, D.M. France, M.W. Wambsganss, J.R. Hull, Two-phase pressure drop, boiling heat transfer, and critical heat flux to water in a small-diameter horizontal tube, Int. J. Multiphase Flow 28 (2002) 927–941.
[36] Y.W. Hwang, M.S. Kim, The pressure drop in microtubes and the correlation development, Int. J. Heat Mass Transfer 49 (2006) 1804–1812.
[37] L. Sun, K. Mishima, Evaluation analysis of prediction methods for two-phase flow pressure drop in mini-channels, Int. J. Multiphase Flow 35 (2009) 47–54.
[38] W. Zhang, T. Hibiki, K. Mishima, Correlations of two-phase frictional pressure drop and void fraction in mini-channel, Int. J. Heat Mass Transfer 53 (2010) 453–465.
[39] W. Li, Z. Wu, Generalized adiabatic pressure drop correlations in evaporative micro/mini-channels, Exp. Therm. Fluid Sci. 35 (2011) 866–872.
[40] W. Qu, I. Mudawar, Measurement and prediction of pressure drop in two-phase micro-channel heat sinks, Int. J. Heat Mass Transfer 46 (2003) 2737–2753.
[41] R.W. Lockhart, R.C. Martinelli, Proposed correlation of data for isothermal two-phase, two-component flow in pipes, Chem. Eng. Prog. 45 (1949) 39–48.
[42] S.M. Kim, I. Mudawar, Review of databases and predictive methods for heat transfer in condensing and boiling mini/micro-channel flows, Int. J. Heat Mass Transfer 77 (2014) 627–652.
[43] M. Ducoulombier, S. Colasson, J. Bonjour, P. Haberschill, Carbon dioxide flow boiling in a single microchannel – Part II: Heat transfer, Exp. Therm. Fluid Sci. 35 (2011) 597–611.
[44] H.K. Oh, C.H. Son, Evaporation flow pattern and heat transfer of R-22 and R-134a in small diameter tubes, Heat Mass Transfer 47 (2011) 703–717.
[45] G.M. Lazarek, S.H. Black, Evaporative heat transfer, pressure drop and critical heat flux in a small vertical tube with R-113, Int. J. Heat Mass Transfer 25 (1982) 945–960.
[46] G.R. Warrier, V.K. Dhir, L.A. Momoda, Heat transfer and pressure drop in narrow rectangular channels, Exp. Therm. Fluid Sci. 26 (2002) 53–64.
[47] B. Agostini, A. Bontemps, Vertical flow boiling of refrigerant R134a in small channels, Int. J. Heat Fluid Flow 26 (2005) 296–306.
[48] W. Li, Z. Wu, A general correlation for evaporative heat transfer in micro/mini-channels, Int. J. Heat Mass Transfer 53 (2010) 1778–1787.
[49] S.M. Kim, I. Mudawar, Theoretical model for local heat transfer coefficient for annular flow boiling in circular mini/micro-channels, Int. J. Heat Mass Transfer 73 (2014) 731–742.
[50] D.D. Hall, I. Mudawar, Ultra-high critical heat flux (CHF) for subcooled water flow boiling – II. High-CHF database and design parameters, Int. J. Heat Mass Transfer 42 (1999) 1429–1456.
[51] T.C. Willingham, I. Mudawar, Forced-convection boiling and critical heat flux from a linear array of discrete heat sources, Int. J. Heat Mass Transfer 35 (1992) 2879–2890.
[52] J.C. Sturgis, I. Mudawar, Critical heat flux in a long, rectangular channel subjected to one-sided heating – II. Analysis of CHF data, Int. J. Heat Mass Transfer 42 (1999) 1849–1862.
[53] H. Zhang, I. Mudawar, M.M. Hasan, Flow boiling CHF in microgravity, Int. J. Heat Mass Transfer 48 (2005) 3107–3118.
[54] J. Lee, I. Mudawar, Two-phase flow in high-heat-flux micro-channel heat sink for refrigeration cooling applications: Part II – Heat transfer characteristics, Int. J. Heat Mass Transfer 48 (2005) 941–955.
[55] J. Lee, I. Mudawar, Low-temperature two-phase micro-channel cooling for high-heat-flux thermal management of defense electronics, IEEE Trans. – CPMT: Compon. Packag. Technol. 32 (2009) 453–465.
[56] J. Lee, I. Mudawar, Critical heat flux for subcooled flow boiling in micro-channel heat sinks, Int. J. Heat Mass Transfer 52 (2009) 3341–3352.
[57] M.B. Bowers, I. Mudawar, Two-phase electronic cooling using mini-channel and micro-channel heat sinks - part 2. Flow rate and pressure drop constraints, J. Electron. Packag. – Trans. ASME 116 (1994) 298–305.
[58] S.M. Kim, I. Mudawar, Review of two-phase critical flow models and investigation of the relationship between choking, premature CHF, and CHF in micro-channel heat sinks, Int. J. Heat Mass Transfer 87 (2015) 497–511.
[59] S.M. Kim, I. Mudawar, Universal approach to predicting two-phase frictional pressure drop for mini/micro-channel saturated flow boiling, Int. J. Heat Mass Transfer 58 (2013) 718–734.
[60] S.M. Kim, I. Mudawar, Universal approach to predicting saturated flow boiling heat transfer in mini/micro-channels – Part I. Dryout incipience quality, Int. J. Heat Mass Transfer 64 (2013) 1226–1238.
[61] S.M. Kim, I. Mudawar, Universal approach to predicting saturated flow boiling heat transfer in mini/micro-channels – Part II. Two-phase heat transfer coefficient, Int. J. Heat Mass Transfer 64 (2013) 1239–1256.
[62] W. Qu, I. Mudawar, Measurement and correlation of critical heat flux in two-phase micro-channel heat sinks, Int. J. Heat Mass Transfer 47 (2004) 2045–2059.
[63] J.G. Collier, J.R. Thome, Convective Boiling and Condensation, third ed., Oxford University Press, New York, NY, 1994.
[64] J. Schmidt, L. Friedel, Two-phase pressure drop across sudden contractions in duct areas, Int. J. Multiphase Flow 23 (1997) 283–299.
[65] F.F. Abdelall, G. Hahn, S.M. Ghiaasiaan, S.I. Abdel-Khalik, S.S. Jeter, M. Yoda, D.L. Sadowski, Pressure drop caused by abrupt flow area changes in small channels, Exp. Therm. Fluid Sci. 29 (2005) 425–434.
[66] S.M. Zivi, Estimation of steady-state steam void-fraction by means of the principle of minimum entropy production, J. Heat Transfer – Trans. ASME 86 (1964) 247–252.
[67] R.K. Shah, A.L. London, Laminar Flow Forced Convection in Ducts: A Source Book for Compact Heat Exchanger Analytical Data, Academic Press, New York, NY, 1978, Supl. 1.
[68] S.M. Kim, I. Mudawar, Universal approach to predicting two-phase frictional pressure drop for adiabatic and condensing mini/micro-channel flows, Int. J. Heat Mass Transfer 55 (2012) 3246–3261.
[69] E.W. Lemmon, M.L. Huber, M.O. McLinden, Reference Fluid Thermodynamic and Transport Properties – REFPROP Version 8.0, NIST, MD, 2007.
[70] F.P. Incropera, D.P. Dewitt, Fundamentals of Heat and Mass Transfer, 5th ed., Wiley, New York, NY, 2002.
[71] G.B. Wallis, One Dimensional Two-Phase Flow, second ed., McGraw-Hill, New York, NY, 1969.
[72] J.A. Shmerler, I. Mudawar, Local heat transfer coefficient in wavy free-falling turbulent liquid films undergoing uniform sensible heating, Int. J. Heat Mass Transfer 31 (1988) 67–77.
[73] J.A. Shmerler, I. Mudawar, Local evaporative heat transfer coefficient in turbulent free-falling liquid films, Int. J. Heat Mass Transfer 31 (1988) 731–742.
[74] T.H. Lyu, I. Mudawar, Statistical investigation of the relationship between interfacial waviness and sensible heat transfer to a falling liquid film, Int. J. Heat Mass Transfer 34 (1991) 1451–1464.
[75] T.H. Lyu, I. Mudawar, Determination of wave-induced fluctuations of wall temperature and convective heat transfer coefficient in the heating of a turbulent falling liquid film, Int. J. Heat Mass Transfer 34 (1991) 2521–2534.
[76] I. Mudawar, R.A. Houpt, Mass and momentum transport in smooth falling liquid films laminarized at relatively high Reynolds numbers, Int. J. Heat Mass Transfer 36 (1993) 3437–3448.
[77] I. Mudawar, R.A. Houpt, Measurement of mass and momentum transport in wavy-laminar falling liquid films, Int. J. Heat Mass Transfer 36 (1993) 4151–4162.
[78] W. Qu, I. Mudawar, S.-Y. Lee, S.T. Wereley, Experimental and computational investigation of flow development and pressure drop in a rectangular micro-channel, J. Electron. Packag. – Trans. ASME 128 (2006) 1–9.